

On the limitations of transmissibility functions for damage localisation: the influence of completeness

Joshua WR Meggitt¹ and Ramin C McGee

Structural Health Monitoring

1–13

© The Author(s) 2024



Article reuse guidelines:

sagepub.com/journals-permissions

DOI: 10.1177/14759217241226602

journals.sagepub.com/home/shm



Abstract

Transmissibility functions are used to identify and locate damage in critical structures for health monitoring purposes. Their appeal over conventional signal or frequency response-based functions lie in a unique property; sub-structural invariance. It has been shown that the transmissibility of an assembled structure, when obtained correctly, can describe the dynamics of a *sub-structure* in a manner that is independent from the remainder of the assembly. It is this sub-structural invariance that enables transmissibility functions to locate damage in complex structures. Though a valuable property, sub-structural invariance relies on the notion of a *complete interface representation*; the interface that separates the sub-structure from the remaining assembly must be sufficiently instrumented so that all important interface dynamics can be captured. In practice, without considerable experimental effort, complete interface representations are not achievable. Importantly, the transmissibilities obtained in the presence of an incomplete interface are unable to discern between damage located interior, or exterior, to a particular sub-structure; they are no longer invariant. Hence, their ability to locate damage is compromised. In the present paper we introduce the notion of completeness in the context of transmissibility-based structural health monitoring, and examine its importance for the accurate localisation of damage through numerical and experimental examples.

Keywords

Damage localisation, transmissibility, sub-structural invariance, completeness, output-only

Introduction

Structural health monitoring (SHM) is a key technology in high-value infrastructure and engineering. There exist two focal applications of SHM; condition monitoring of rotating machinery (e.g. generators, electric drives, etc.), and the assessment of structural integrity (e.g. bridges, buildings, etc.). The present paper will focus on this latter application.

A principle concept that underlies many of the structural analysis-based SHM methods is that damage alters the dynamic properties of a structure, typically through a reduction of stiffness.¹ By developing indicators, or metrics, that are sensitive to the effect of these changes (e.g. shifts in natural frequencies, changes in mode shapes, etc.), SHM attempts to answer one or more of the following questions²: Does damage exist? (Detection); Where is the damage? (Localisation); How serious is the damage? (Assessment); How long will the structure remain operational? (Prediction). SHM indicators are often obtained by comparing the experimental response (or extracted features) of a structure, to

those of a numerical counter part. A challenge here is to build an accurate model of the initial structure. Alternatively, comparisons can be made against a baseline result obtained during commissioning.

When developing an SHM indicator, it is important to choose the right features for comparison. To aid the localisation of damage, chosen features should be local in nature, that is, unaffected by damage located far away.³ Of the available features, and of principle interest in the present paper, is the transmissibility function which, when obtained correctly, can provide localised (i.e. sub-structural) information on the dynamic properties of a structure.⁴ This unique property of the transmissibility function, termed sub-structural invariance,

Acoustics Research Centre, University of Salford, Salford, Greater Manchester, UK

Corresponding author:

Joshua WR Meggitt, Acoustics Research Centre, University of Salford, 43 Crescent, Salford, Greater Manchester, M5 4WT, UK.

Email: j.w.r.meggitt1@salford.ac.uk

though a requirement for damage localisation, is not a guaranteed property. Rather, it relies on what is termed a *complete interface representation*.⁵

To benefit from the invariance properties of the transmissibility, the interfaces that separate each sub-structure from the remaining assembly must be instrumented such that all important interface dynamics can be captured. For practical engineering structures, where many sub-structures and connection points are present, a complete representation of all interfaces is not achievable. An important consequence of which is that the transmissibilities obtained are no longer invariant. Hence, their ability to locate damage is compromised.

In the present paper we introduce the Interface Completeness Criterion (ICC)⁵ as a quantitative measure of interface completeness, and investigate its correlation with the localisation capability of transmissibility-based damage metrics. Through a series of numerical and experimental examples it is shown that for a sufficiently complete interface representation, transmissibility-based metrics have the potential to provide a reliable localisation of damage. In contrast, with an incomplete representation the same metrics are unable to localise damage with any confidence, often attributing it to the wrong sub-structure.

Having introduced the context of this paper, its remainder will be structured as follows. Section ‘Transmissibility: a sub-structural invariant’ will begin by introducing the transmissibility and its invariant sub-structural properties, also discussing its application in the context of SHM. Section ‘Completeness’ introduces the notion of completeness, and outlines its quantification (the ICC). In section ‘Numerical study: connected plates’ we consider a numerical example in which two plates (one subject to simulated damage) are connected by a continuous interface, of which different levels of discretisation (i.e. completeness) are considered. In section ‘Experimental study: connected beams’ a similar study is performed, though experimentally with beam-like components coupled via point-like connections. Finally, section ‘Conclusion’ draws some concluding remarks.

Transmissibility: a sub-structural invariant

Generally, a transmissibility describes the relation between two like quantities. The most common transmissibilities are those of force and response (taken to be displacement, velocity or acceleration). The force transmissibility T_{ij}^f is defined here as the relation between an applied force f_j at the DoF j , and the blocking force $-\bar{f}_i$ at the DoF i (i.e. the forces required to

constrain the response $u_i = 0$, see Moorhouse et al.⁶ and Meggitt⁷ for more details), whilst all other forces are subject to a zero force constraint $f_{k \neq j} = 0$,

$$\begin{pmatrix} -\bar{f}_1 \\ \vdots \\ -\bar{f}_N \end{pmatrix} = \begin{bmatrix} T_{11}^f & \cdots & T_{1M}^f \\ \vdots & \ddots & \vdots \\ T_{N1}^f & \cdots & T_{NM}^f \end{bmatrix} \begin{pmatrix} f_1 \\ \vdots \\ f_M \end{pmatrix}, \quad (1)$$

$$T_{ij}^f = \left. \frac{-\bar{f}_i}{f_j} \right|_{f_{k \neq j} = 0}$$

Note that the excitation and blocking force DoFs belong to different sets of measurement positions ($j \in M$ and $i \in N$), and that if several blocking DoFs are considered, a constraint is applied to all, $u_{i \in N} = 0$.

The response transmissibility T_{ij}^d describes the relation between the response u_j at DoF j , and the response u_i at DoF i , due to the applied force f , whilst all other DoFs are subject to a rigid constraint $u_{k \neq j} = 0$,

$$\begin{pmatrix} u_1 \\ \vdots \\ u_M \end{pmatrix} = \begin{bmatrix} T_{11}^d & \cdots & T_{1N}^d \\ \vdots & \ddots & \vdots \\ T_{M1}^d & \cdots & T_{MN}^d \end{bmatrix} \begin{pmatrix} u_1 \\ \vdots \\ u_N \end{pmatrix}, \quad (2)$$

$$T_{ij}^d = \left. \frac{u_i}{u_j} \right|_{u_{k \neq j} = 0}$$

where again, the two response DoFs belong to different sets ($j \in N$ and $i \in M$).

From the above it is clear that there exists a symmetry between the force and response transmissibility. Defined in terms of a blocking force, implicit to the force transmissibility are a set of rigid constraints. Similarly, by definition the response transmissibility requires the rigid constraint of all DoFs $k \neq j$.

The invariant nature of the transmissibility arises due to the blocking constraints present in the above definitions. If these blocking constraints are applied to the DoFs that separate a sub-structure from the remainder of its assembly, the dynamics of neighbouring sub-structures are effectively removed, and so they become invariant sub-structural properties. It is this invariance that enables, in theory, transmissibility-based metrics to localise damage.

Force transmissibility

We begin by considering the coupled AB assembly in Figure 1(a), though what follows may be generalised to more complex arrangements of sub-structures. Two sets of DoFs are considered; the remote set a , located internal to sub-structure A , and the interface set c . According to the equivalent field theorem,^{6,8} the response field along the interface c generated by an

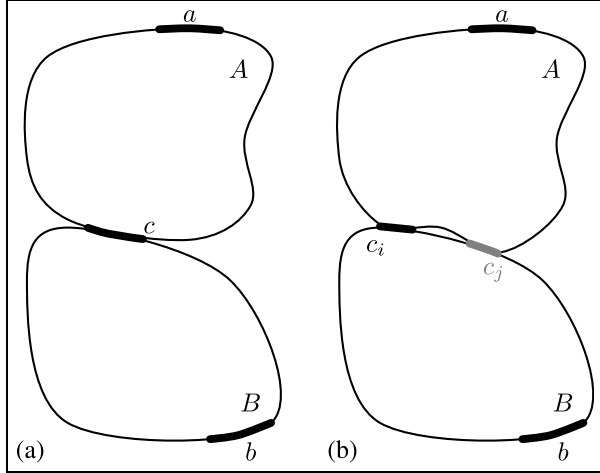


Figure 1. Interface representations of coupled structures: (a) single complete interface and (b) interface with known (c_i) and unknown (c_j) DoFs.

external force \mathbf{f}_a can be reproduced identically by applying the (negative) blocking force $-\bar{\mathbf{f}}_{Ac}$ in place of the original excitation. We thus have the following equality,

$$\mathbf{u}_c = \mathbf{Y}_{Cca}\mathbf{f}_a = -\mathbf{Y}_{Ccc}\bar{\mathbf{f}}_{Ac} \quad (3)$$

where \mathbf{Y}_{Cca} is the transfer receptance matrix of the coupled assembly $C=AB$ from the internal DoFs a to the coupling interface c , and \mathbf{Y}_{Ccc} is the point receptance matrix of the coupled assembly at the interface c . Pre-multiplying both sides of Equation (3) by the inverse receptance matrix \mathbf{Y}_{Ccc}^{-1} then yields,

$$-\bar{\mathbf{f}}_{Ac} = \mathbf{Y}_{Ccc}^{-1}\mathbf{Y}_{Cca}\mathbf{f}_a. \quad (4)$$

Like Equation (1), Equation (4) relates the applied force \mathbf{f}_a to the blocking force $-\bar{\mathbf{f}}_{Ac}$. We can thus identify the force transmissibility as,

$$\mathbf{T}_{Aca}^f = \mathbf{Y}_{Ccc}^{-1}\mathbf{Y}_{Cca}. \quad (5)$$

It is significant that the above definition of force transmissibility is based entirely on *coupled* assembly receptances. The force transmissibility \mathbf{T}_{Aca}^f is therefore a sub-structure invariant available from in-situ experimental testing; its invariance, being a consequence of the blocking constraint ($\bar{\mathbf{f}}_{Ac}$) in its definition.⁴

Response transmissibility

Turning attention towards the response transmissibility, we consider the application of an external force at the interface c (as opposed to a as used in the force

transmissibility). The response at the interface and internal DoFs are given, respectively, by

$$\mathbf{u}_c = \mathbf{Y}_{Ccc}\mathbf{f}_c \quad (6)$$

and

$$\mathbf{u}_a = \mathbf{Y}_{Cac}\mathbf{f}_c. \quad (7)$$

Rearranging Equation (6) to determine \mathbf{f}_c and substituting this into Equation (7) leads to the response transmissibility relation,

$$\mathbf{u}_a = \mathbf{Y}_{Cac}\mathbf{Y}_{Ccc}^{-1}\mathbf{u}_c = \mathbf{T}_{Aac}^d\mathbf{u}_c \quad (8)$$

where,

$$\mathbf{T}_{Aac}^d = \mathbf{Y}_{Cac}\mathbf{Y}_{Ccc}^{-1}. \quad (9)$$

At first sight it is not obvious that the response transmissibility is also a sub-structural invariant. This is made clearer by considering the nature of the external force \mathbf{f}_c . The dynamic influence of sub-structure B onto A (i.e. due to internal coupling forces) can be represented by an appropriate external force \mathbf{f}_c , on which no requirements were placed in the derivation of Equation (8). Hence, Equation (8) is valid in the presence of an arbitrary forcing term, and so the response transmissibility \mathbf{T}_{Aac}^d is an invariant sub-structural property.

Inspection of Equations (5) and (9) reveals that the force and response transmissibility are related. Here, as we have reversed the direction of the response transmissibility (it goes from c to a , rather than a to c like the force transmissibility), we have that,

$$\mathbf{T}_{Aca}^f = \mathbf{Y}_{Ccc}^{-1}\mathbf{Y}_{Cca} = (\mathbf{Y}_{Cac}\mathbf{Y}_{Ccc}^{-1})^T = (\mathbf{T}_{Aac}^d)^T \quad (10)$$

That is, the force transmissibility is equal to the transposed response transmissibility, both of which are invariant sub-structural properties. Note that in Lage et al.⁹ and Meggitt and Moorhouse⁴ the direction of the response transmissibility is not reversed, and so their relations include an inverse.

Note that by considering an additional set of internal DoFs b located on sub-structure B , the force or response transmissibility $\mathbf{T}_{Bbc}^{f,d}$ can be obtained by simply interchanging sub-scripts $a \rightarrow b$. Further extension to include additional sub-structures is achieved by simply defining appropriate sets of interface DoFs that enclose each sub-structure.

In the above, both force and response transmissibilities are defined in terms of coupled assembly receptances (or more generally, structural frequency response functions (FRFs)). Whilst these FRFs are readily measurable quantities, requiring a known input force and measured response (most often an acceleration), in the context of SHM their measurement can be

impractical as it requires human intervention to measure \mathbf{Y}_{Ccc} and \mathbf{Y}_{Cca} (or \mathbf{Y}_{Cac}). Instead, it is possible to define the transmissibility in terms of output-only quantities.

Output-only transmissibility

Suppose sub-structure A is installed within an active assembly, that is, an assembly containing one or more vibration generating mechanisms. In this case it is possible to determine the transmissibility based on measurements of the operational response only. A key requirement of the above is that the vibration generating mechanisms do not reside within the target sub-structure, as the ‘excitation’ DoFs (taken here to be those of the interface c) must be known and instrumented.

To extend the definition of transmissibility to output-only quantities it is sufficient to consider N linearly independent operational states of the assembly AB . From the perspective of sub-structure A , each operational state can be represented by an external force $\mathbf{f}_c^{(i)}$. Arranging the external force vectors as the columns of a matrix we arrive at the external force matrix $\mathbf{F}_c = [\mathbf{f}_c^{(1)} \ \dots \ \mathbf{f}_c^{(N)}]$. Equations (6) and (7) can thus be rewritten as,

$$\mathbf{U}_c = \mathbf{Y}_{Ccc} \mathbf{F}_c \quad (11)$$

and

$$\mathbf{U}_a = \mathbf{Y}_{Cac} \mathbf{F}_c \quad (12)$$

and Equation (8) as,

$$\mathbf{U}_a = \mathbf{Y}_{Cac} \mathbf{Y}_{Ccc}^{-1} \mathbf{U}_c, \quad (13)$$

where \mathbf{U}_c and \mathbf{U}_a represent operational response matrices at, respectively, the interface and internal DoFs of sub-structure A . From Equation (13) it is straightforward to identify the response transmissibility matrix,

$$\mathbf{T}_{Aac}^d = \mathbf{Y}_{Cac} \mathbf{Y}_{Ccc}^{-1} = \mathbf{U}_a \mathbf{U}_c^{-1}. \quad (14)$$

Similarly, using Equation (10) we can define the force transmissibility matrix as,

$$\mathbf{T}_{Aac}^f = (\mathbf{U}_a \mathbf{U}_c^{-1})^T = \mathbf{U}_c^{-T} \mathbf{U}_a^T. \quad (15)$$

Equations (14) and (15) provide output-only definitions of the sub-structure transmissibilities \mathbf{T}_{Aac}^d and \mathbf{T}_{Aac}^f , respectively, requiring measurement of the operational response only. Note however, that to determine the transmissibility by means of output only measurements, as per Equations (14) and (15), the inverted response matrix must be of full rank (each operational

state must produce a linearly independent response), or preferably over-determined.^{10,11}

The transmissibilities obtained as per Equations (5), (9), (14) or (15) are often termed ‘global’ or ‘generalised’ transmissibilities. In contrast, the transmissibilities used most often in SHM are termed ‘local’ and are defined as the *scalar* ratio of responses,

$$T_{ij}^d = \frac{u_i}{u_j}. \quad (16)$$

Note that this local transmissibility does not benefit from the rigid constraints present in Equation (2). Consequently, it does not provide an invariant sub-structural property. For this reason, local transmissibilities are not suitable for damage localisation.

Transmissibility-based damage metrics

In the above, it was shown that the transmissibility, when defined between a set of internal and interface DoFs, is indeed a sub-structural invariant. Furthermore, being a product of receptance functions, the transmissibility (force or response) is also sensitive to changes in the mass, stiffness or damping distribution of a structure.¹² In combination, these invariance and sensitivity properties enable the localisation of damage using transmissibility functions; the transmissibility of a sub-structure is only changed if damage occurs *within* that sub-structure, damage located outside that sub-structure will have no effect on its transmissibility. To the authors’ knowledge, this is the first definitive and general explanation as to why transmissibilities are able to localise damage.

Since their first use in the context of SHM,¹³ various transmissibility-based metrics have been proposed to quantify the level of damage present in a structure or sub-structure, including difference-based,^{3,12,14–18} correlation-based^{19–21} and coherence-based²² formulations. Irrespective of their formulation, the general idea is that the corresponding damage metric describes the similarity between a baseline (undamaged) transmissibility $\mathbf{T}_{\square}^{(b)}$, obtained either by measurement or modelling, and that of a potentially damaged structure $\mathbf{T}_{\square}^{(d)}$.

Completeness

In our treatment of transmissibility we considered sub-structure A , whose interface was represented completely by the DoF set c . Owing to its implicit constraints, the transmissibility $\mathbf{T}_{Aca}^{f,d}$ effectively removes the influence of sub-structure B by constraining all interface DoFs. In the context of SHM, the transmissibility $\mathbf{T}_{Aca}^{f,d}$ is invariant to damage within sub-structure B , whilst sensitive to damage within sub-structure A .

This invariance can, in theory, be used to identify and attribute damage to a specific sub-structure within an assembly.

Now suppose we consider the coupled AB assembly depicted in Figure 1(b), where the interface DoFs c are separated into *measurable* DoFs c_i , and *inaccessible* DoFs c_j . The transmissibility obtained by considering the measurable DoFs c_i constrains only the c_i DoFs; the remaining c_j DoFs are left unconstrained. Hence, sub-structure B remains ‘coupled’ to sub-structure A , and the transmissibility obtained belongs to the AB assembly, $\mathbf{T}_{ABc_i a}^{f,d}$ (see Appendix A for details). In the context of SHM, the transmissibility $\mathbf{T}_{ABc_i a}^{f,d}$ is sensitive to damage within both sub-structure A and B ; therefore it cannot be used to attribute damage to either.

If the intention is to use a standard transmissibility-based metric to identify or locate damage within an assembly, complete interface representations are required, else damage may falsely be attributed to the wrong sub-structure.

Quantifying completeness

Experimentally, an interface representation describes the number, and orientation, of response sensors used to instrument an interface. Completeness describes the ability of the installed sensor array to capture the full range of dynamics, or DoFs, at the interface. The DoFs that are physically present at an interface form two subsets; those that are known and measurable, and those that are unknown, or known but cannot be measured (e.g. due to poor access, or limited instrumentation). It is the presence of this latter subset that gives rise to incompleteness.

The notion of interface completeness was first introduced by Meggitt and Moorhouse⁵ in the context of vibration source characterisation. It was shown that by neglecting a subset of interface DoFs, a bias error (or model uncertainty) is introduced that renders the source characterisation structurally dependent (as opposed to invariant). To quantify the severity of incompleteness, they considered mathematically blocking the known (measurable) interface DoFs, and observing the response obtained downstream of the interface when an upstream excitation is applied; in the presence of a complete interface representation, the interface is completely blocked and the observed response is zero; in the presence of an incomplete interface, some response will be observed due to propagation through the unconstrained (unknown) DoFs.

It was shown that the blocking ability of an interface representation can be assessed through the comparison of two receptance matrices that traverse the interface. With reference to Figure 1(b), the first is a directly measured receptance $\mathbf{Y}_{Cab}^{(c)}$, and the second is a (round

trip²³) reconstructed receptance $\mathbf{Y}_{Cab}^{(c_i)} = \mathbf{Y}_{Cac_i} \mathbf{Y}_{Cc_i c_i}^{-1} \mathbf{Y}_{Cc_i b}$ that takes into account only the known measurable DoFs c_i . In the presence of a complete interface representation, these two transfer receptances are equal,

$$\mathbf{Y}_{Cab}^{(c)} = \mathbf{Y}_{Cab}^{(c_i)} = \mathbf{Y}_{Cac_i} \mathbf{Y}_{Cc_i c_i}^{-1} \mathbf{Y}_{Cc_i b}. \quad (17)$$

Hence, to quantify completeness, it is sufficient to assess the similarity of the direct and reconstructed receptances above. To this end, Meggitt and Moorhouse adopted a correlation-based measure of similarity and proposed the so-called Interface Completeness Criterion (ICC),

$$\text{ICC} = \text{Corr}(\mathbf{Y}_{Cab}^{(c)}, \mathbf{Y}_{Cab}^{(c_i)}) \quad (18)$$

$$\text{Corr}(\mathbf{a}, \mathbf{b}) = \frac{|\mathbf{a}^H \mathbf{b}|^2}{\mathbf{a}^H \mathbf{a} \cdot \mathbf{b}^H \mathbf{b}} \quad (19)$$

where \square denotes matrix column-wise vectorisation and \square^H represents a conjugate transpose. Note that to form the necessary vectors multiple excitation and/or response DoFs (b and a) should be considered when measuring the necessary FRFs.

An alternative measure of similarity has also been proposed based on a coherence style formulation,²⁴

$$\text{ICC} = \langle \text{ICC}_{nm} \rangle \quad (20)$$

$$\text{ICC}_{nm} = \text{Coh}(\mathbf{Y}_{Ca_n b_m}^{(c)}, \mathbf{Y}_{Ca_n b_m}^{(c_i)}) \quad (21)$$

$$\text{Coh}(a, b) = \frac{(a+b)(a^*+b^*)}{2(aa^*+bb^*)} \quad (22)$$

where \square^* denotes complex conjugate and $\langle \square \rangle$ an average over the indices nm .

In the presence of a complete interface representation $c = c_i$, $\mathbf{Y}_{Cab}^{(c)} = \mathbf{Y}_{Cab}^{(c_i)}$, and the above ICCs are equal to 1. If any DoFs are omitted, this equality is not satisfied and the ICCs yield values less than 1.

To obtain the ICC, the receptances \mathbf{Y}_{Cac_i} , $\mathbf{Y}_{Cc_i c_i}$, $\mathbf{Y}_{Cc_i b}$ and \mathbf{Y}_{Cab} should be measured. This requires response instrumentation of the known interface c_i and remote a DoFs. This level of instrumentation might be expected for a typical output only SHM exercise. Excitations are also applied to known interface c_i and remote b DoFs. These excitations constitute the additional experimental effort required to determine the ICC over a conventional SHM exercise, and would be applied during commissioning.

Importantly, the ICC is a frequency dependent quantity; the contribution of each interface DoF varies with frequency depending on the modal characteristics of the structure. At certain frequencies the interface may be represented adequately using only a small subset of the DoFs present. At others, a greater number,

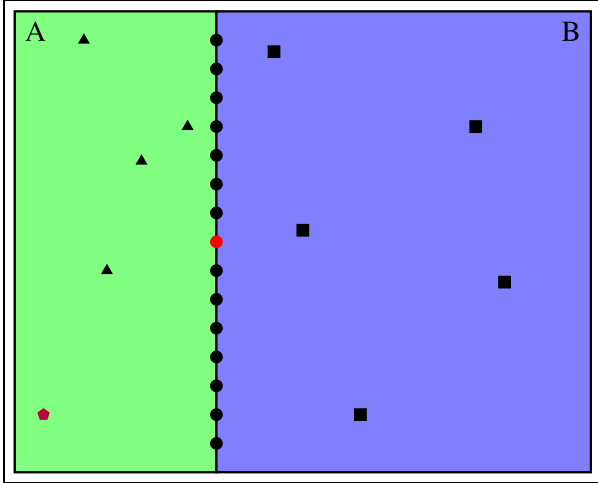


Figure 2. Diagram of coupled plate simulation; two plates (A and B) coupled along a continuous interface. Markers: \blacktriangle – remote A DoFs, \blacksquare – remote B DoFs, \bullet – discretised interface DoFs (\bullet – is a fixed interface DoF used for all levels of discretisation), \blacksquare – location of added mass/damage.

or a different subset, may be required. Given an interface representation, the ICC indicates over what frequency range(s) the interface appears complete, and over which results should not be relied upon.

Numerical study: connected plates

In this section we investigate the influence of interface completeness on the localisation and quantification of damage for a simulated example. The case considered is illustrated in Figure 2.

Two plates (A and B) are coupled along a continuous line. Damage is simulated in plate A by adding a localised mass (approx 10% of total plate mass). Transmissibilities are obtained between a discretised representation of the separating interface c and a set of remote DoFs a and b , located respectively in substructures A and B. The level of interface discretisation is varied and the transmissibilities obtained from the baseline, $\mathbf{T}_{\square}^{(b)}$, and damaged, $\mathbf{T}_{\square}^{(d)}$, systems are used to calculate the following correlation-based damaged metric,

$$D_{\square} = 1 - \frac{1}{f_2 - f_1} \int_{f_1}^{f_2} \text{Corr}(\mathbf{T}_{\square}^{(d)}, \mathbf{T}_{\square}^{(b)}) df \quad (23)$$

where \square denotes vectorisation of the above matrix and $\text{Corr}(\square, \square)$ is the correlation function detailed in Equation (19). A value of $D_{\square} = 0$ indicates no damage, whilst $D_{\square} > 0$ indicates some level of damage, typically

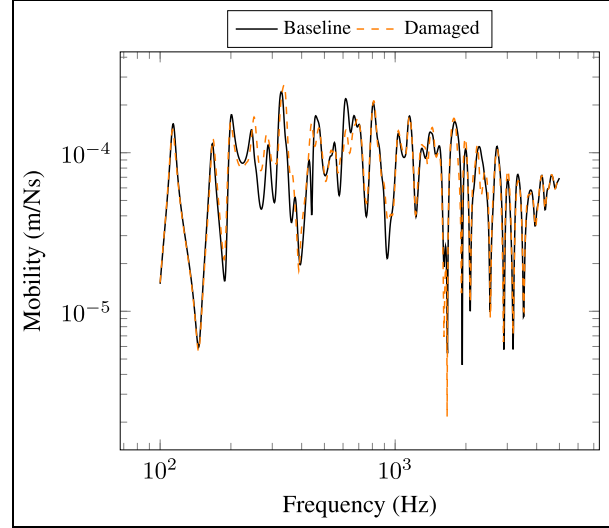


Figure 3. Example transfer mobilities Y_{ab} obtained from the baseline and damaged systems.

with greater values of D_{\square} being attributed to greater levels of damage.

The coupled plate is simulated using a modal summation approach with a simply supported boundary. Each marker shown in Figure 2 represents three DoFs, a vertical translation (z) and a pair of x/y rotations (α/β). The continuous interface is represented by a discretised set of points (each with three DoFs). The level of discretisation and the DoFs included (i.e. with/without rotations), will be varied to alter the completeness of the interface. An example of a baseline and damaged mobility, due to the added mass, is shown in Figure 3.

Shown in Figure 4(a) are the correlation-based ICCs obtained by increasing the level of discretisation through 1, 3, 5, 9 and 15 points (each with three DoFs). In Figure 4(b) are the resulting transmissibilities between a fixed interface point (red marker in Figure 2) and a remote a DoF. It is clear that as the number of points is increased, the completeness of the interface does so also. It is seen that the transmissibility obtained also depends strongly on the level of interface completeness.

Shown in Figure 5 are the ICCs obtained for the full 15 point discretisation, with and without the rotational DoFs included. In contrast to Figure 4(a) which shows a gradual increase in the frequency range that is approx. complete, neglecting rotational DoFs leads to a reduced level of completeness across the entire frequency range.

To illustrate the importance of interface completeness from a damage localisation/quantification standpoint, we consider this latter case (15 points with/without rotations) and compute the transmissibilities

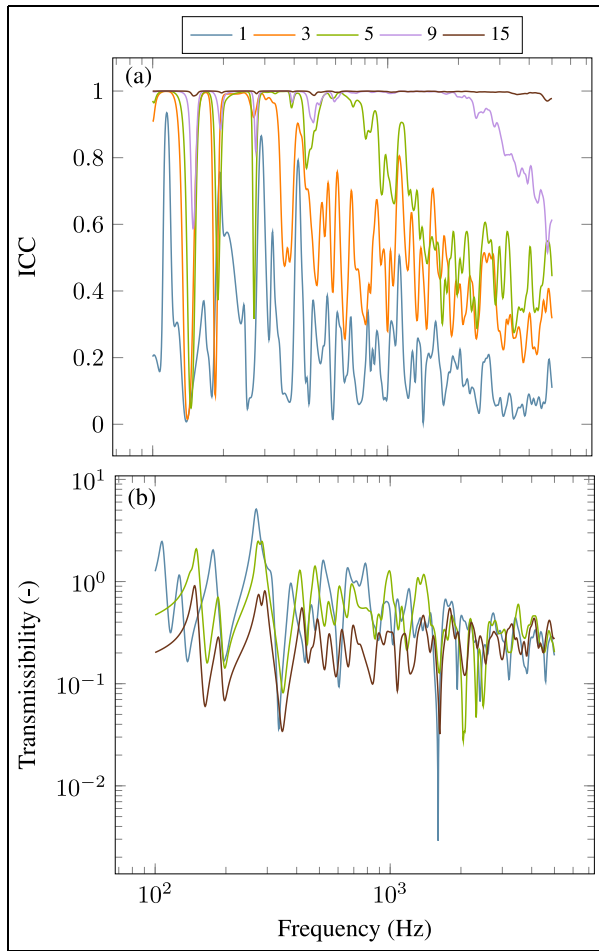


Figure 4. Interface completeness (a) and transmissibility (b) as a function of frequency and number of interface DoFs employed. For clarity, interface representations 3 and 9 have been omitted from (b).

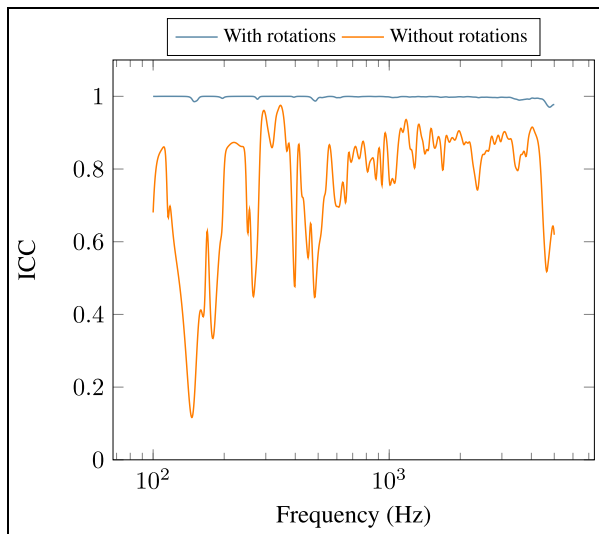


Figure 5. Interface completeness with 15 points, with and without rotations.

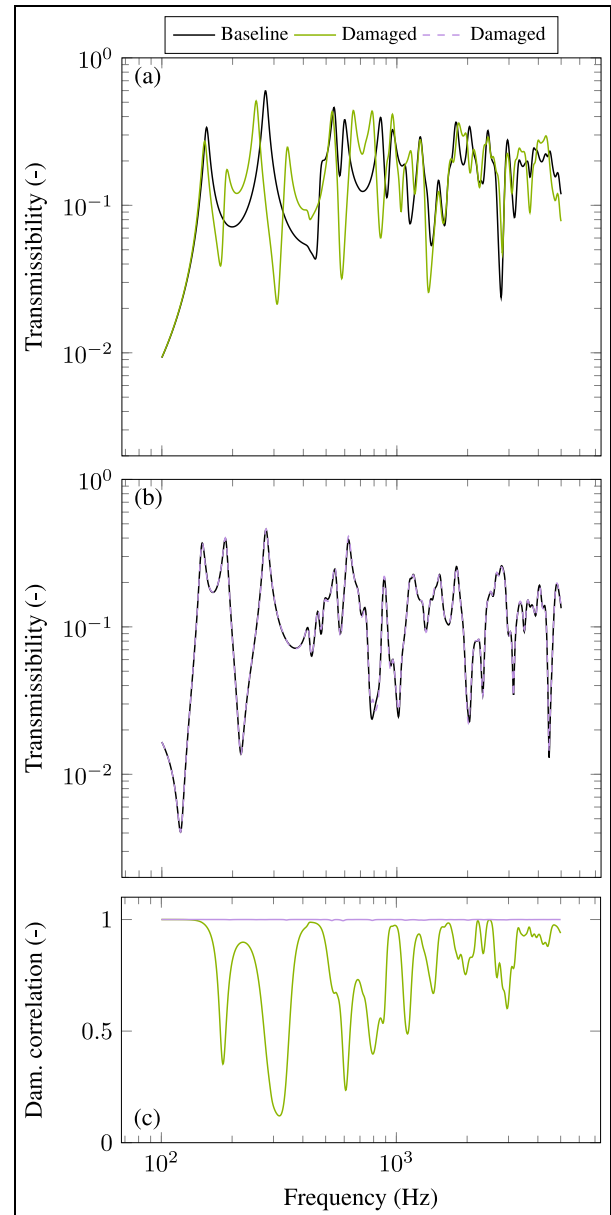


Figure 6. Example transmissibilities of component A (a) and B (b) for baseline and damaged systems with complete interface representation. Also shown in (c) is the damage correlation metric obtained using all transmissibilities. Single value damage metric (see Equation (23)): $D_A = 0.158$, $D_B = 0.0006$.

of sub-structures *A* and *B* for the baseline and damaged cases. For the complete interface (i.e. with rotations) these results are shown in Figure 6. Figure 6(a) shows that the transmissibility of sub-structure *A* is clearly effected[AQ: 5] by the damage located in *A*. Figure 6(b) shows that the transmissibility of sub-structure *B* is completely unaffected by the damage in *A* (note that due to the finite discretisation of the interface, some very small deviations are still seen).

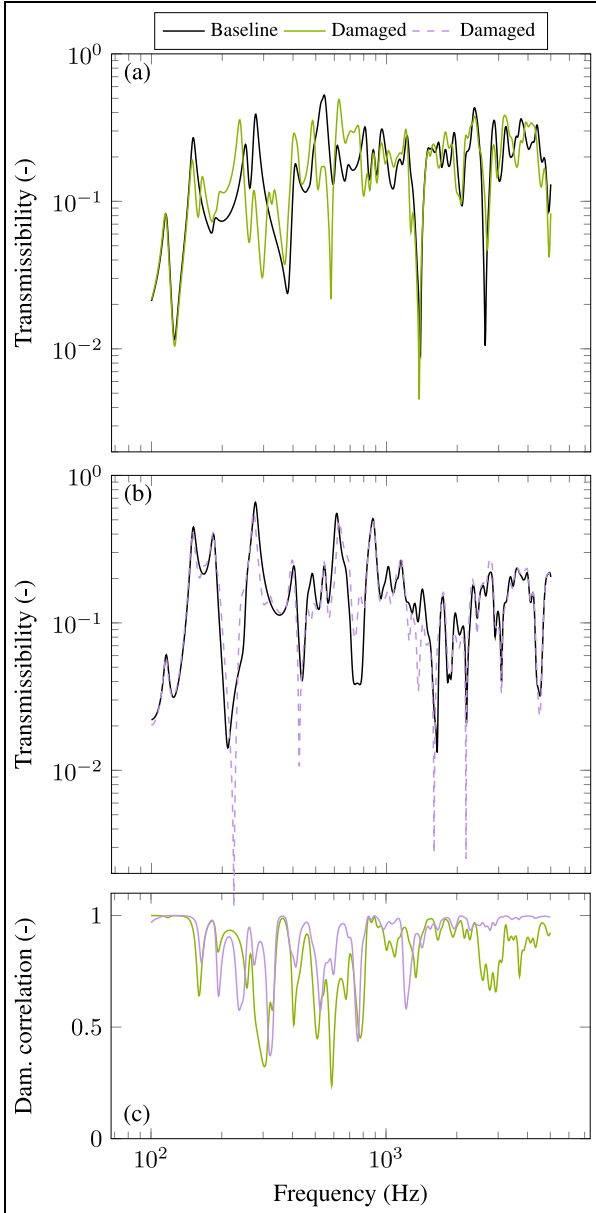


Figure 7. Example transmissibilities of component A (a) and B (b) for baseline and damaged systems with *incomplete* interface representation. Also shown in (c) is the damage correlation metric obtained using all transmissibilities. Single value damage metric (see Equation (23)): $D_A = 0.143$, $D_B = 0.053$.

Recalling that the sub-structure transmissibilities are in fact matrices, a correlation-based comparison can be made between the baseline and damaged cases for A and B ,

$$\text{Dam. corr.} = \text{Corr}(\mathbf{T}_{\square}^{(d)}, \mathbf{T}_{\square}^{(b)}). \quad (24)$$

This result is shown in Figure 6(c). Sub-structure B , being unaffected by the damage, is near perfectly correlated with the undamaged case, whilst sub-structure A

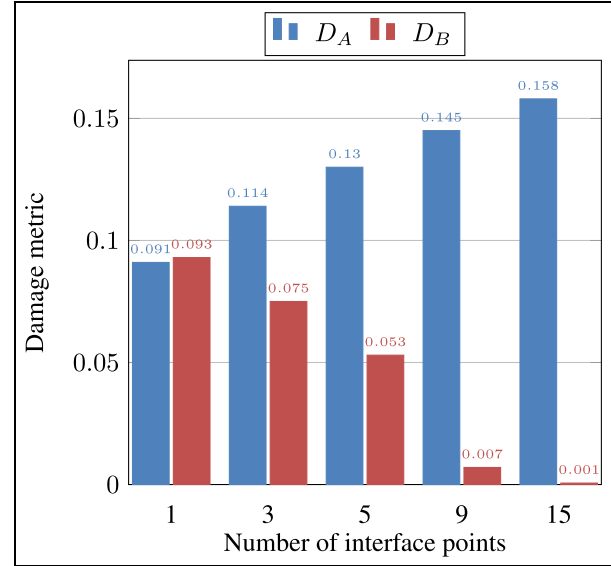


Figure 8. Single value damage metrics for sub-structures A and B (with damage located in A) for increasing levels of interface discretisation.

is not. Taking a shifted frequency average (as per Equation (23)) of this correlation yields the following single value damage metrics (with $f_1 = 100$ and $f_2 = 5000$): $D_A = 0.158$, $D_B = 0.0006$, which clearly identify the location and relative severity of the damage present.

Shown in Figure 7 are an equivalent set of results (as in Figure 6), though obtained from an incomplete interface representation, where rotational interface DoFs have been omitted. As before, the transmissibility of sub-structure A has been effected by the damage, but in this case so has that of sub-structure B . By neglecting the rotational DoFs at the interface, damage in sub-structure A is appearing also as damage in sub-structure B . The results of the correlation-based comparison illustrate this result more generally across the entire transmissibility matrix. The single value damage metrics obtained from Figure 7(c) are: $D_A = 0.143$, $D_B = 0.05$, that is, a reduction in D_A and an approx. $100 \times$ increase in D_B .

Though the single value metrics still suggest sub-structure A to be the more likely origin of damage, this is not necessarily the case for different interface representations (i.e. levels of completeness). This fact can be illustrated by considering the damage metrics obtained as one increases the number of points used to discretise the interface (as illustrate by Figure 4). Shown in Figure 8 are the single value damage metrics obtained for sub-structures A and B for an increasing number of interface points.

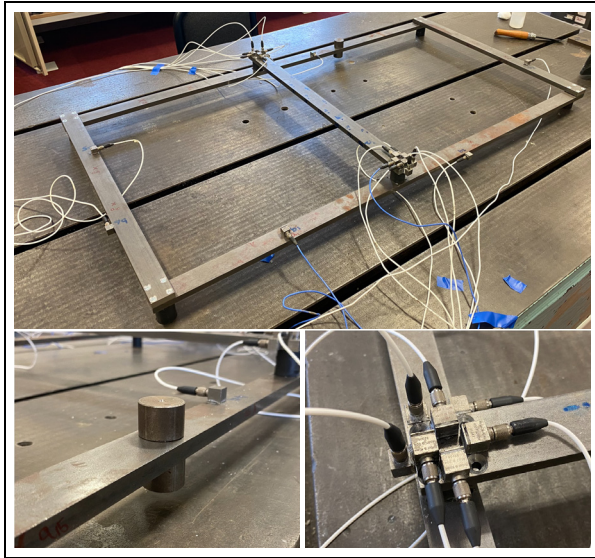


Figure 9. Photo of experimental structure with resilient connection (top), added mass (bottom left) and interface instrumentation (bottom right).

The trends observed in Figure 8 represent main the contribution of this paper. For a high level of interface completeness (15 points), transmissibilities are able to accurately locate damage, as illustrated by the clear separation between D_A and D_B . As the level of completeness is reduced (in this case towards a single point with three DoFs) D_A and D_B begin to converge and no clear distinction can be made. In fact, for the specific case considered here, results suggest that there is a greater level of damage in sub-structure B than A (albeit only marginally). Hence, the ability of transmissibility functions to accurately locate damage is directly proportional to the level of completeness achieved by the given interface representation.

Experimental study: connected beams

In this section we will investigate the robustness of transmissibility-based damage localisation on a more conventional point-like separating interface. The structure under study is shown in Figure 9; a beam component (A) is connected to a frame-like structure (B) composed of four beams bolted together. We consider both a rigid and resilient (i.e. vibration isolated) coupling between the two components. For each, we measure the transmissibilities \mathbf{T}_{Aca} and \mathbf{T}_{Bcb} between the interface c and a set of remote a and b DoFs (located, respectively, on A and B). These transmissibilities are measured for the baseline (undamaged) $\mathbf{T}_{\square}^{(b)}$ and damaged $\mathbf{T}_{\square}^{(d)}$ cases. As before, damage is simulated by adding a small mass, this time to B (mass weight is approx

1.2% of the total system weight). For each scenario, the transmissibility and its corresponding single value damage metric D_{\square} is computed for following interface representations r_n (with decreasing levels of completeness):

- r_1 – all six DoFs (i.e. including the rotational z DoF),
- r_2 – vertical z , and x/y rotations,
- r_3 – vertical z , and in-plane x and y ,
- r_4 – vertical z DoFs only,
- $r_{5,2}$ – single vertical DoF only.

Note that the transmissibilities obtained using the $r_{5,2}$ representations involve the inversion of scalar interface mobility terms (as opposed to a mobility matrices). As such, the resulting transmissibilities are simply direct transmissibilities, defined according to Equation (16). The direct transmissibilities do not possess any rigid constraints in their definition.

Shown in Figure 9 is a photo of the instrumented interface – seven uniaxial accelerometers and seven applied forces are used (per connection) to measure the coupled interface mobility matrix $\mathbf{Y}_{cc} \in \mathbb{C}^{14 \times 14}$. To obtain collocated force and response measurements, excitations were applied directly to each accelerometer. The measurement coherence was monitored to ensure good quality data was obtained and overloading avoided. A finite difference (FD) transformation is applied to extract averaged translational and rotational motions,²⁵ and build the FD interface mobility matrix $\mathbf{Y}_{cc}^{(FD)} \in \mathbb{C}^{12 \times 12}$ (note, the FD approx. is also used to build $\mathbf{Y}_{ca}^{(FD)} \in \mathbb{C}^{12 \times 6}$ and $\mathbf{Y}_{cb}^{(FD)} \in \mathbb{C}^{12 \times 6}$, where the remote DoF positions are chosen arbitrarily). The various interface representations r_n are obtained by simply omitting the appropriate rows and columns from these FD mobility matrices. All measurements are made using B&K type 4507-B accelerometers, a PCB type 086C02 modal hammer, and a DEWEsoft SIRUS acquisition system.

Shown in Figure 10 is an example of the FD mobility in the vertical z direction at one interface connection point for the baseline and damaged case. It is clear from this result that the structure's FRF is most affected in the high frequency regime. To give the damage localisation the best chance of success, the single value damage metric will be obtained using the frequency limits $f_1 = 500$ and $f_2 = 2000$. Note, exactly how to choose appropriate frequency limits for damage metric evaluation is an ongoing question, and further discussion/investigation is beyond the scope of this work.

Shown in Figure 11 are the ICCs for each of the representations, over the chosen frequency range, for the rigidly coupled case. These results suggest that r_1 and r_2 provide similar and reasonable levels of completeness, whilst r_3 and r_4 do not.

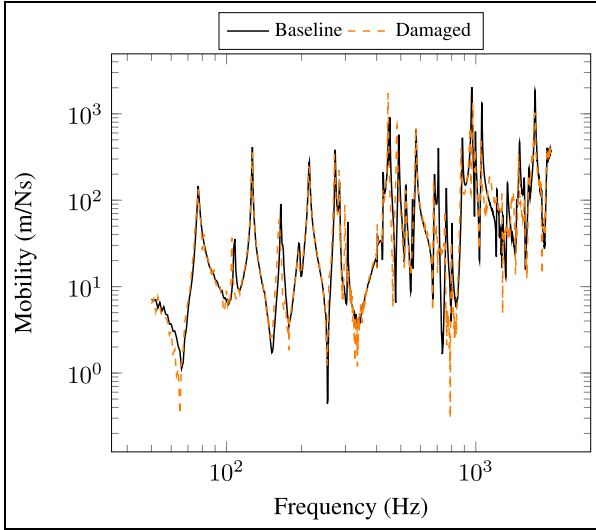


Figure 10. Example point mobilities Y_{cc} obtained from the baseline and damaged structures.

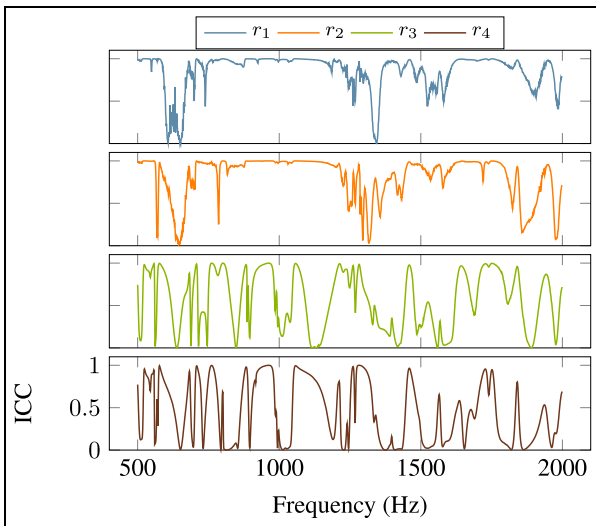


Figure 11. Interface completeness obtained for each representation r_n for the rigidly coupled case.

Shown in Figure 12 are the single value damage metrics obtained for A and B , whilst rigidly coupled, using the various interface representations described above. In all cases the damage was located in B . Before discussing the results however, it is important to note that the calculation of transmissibility requires the inversion of an interface mobility matrix Y_{cc} , and that this can be a very sensitive operation with experimental data, especially for structures with low damping; matrix inversions are known to amplify errors.²⁶ To alleviate this issue a small amount of regularisation (singular

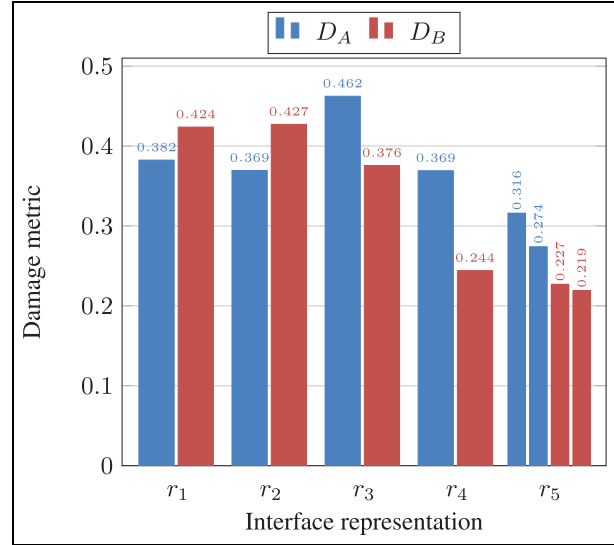


Figure 12. Single value damage metrics for sub-structures A and B (rigidly coupled with damage located in B) for different interface representations.

value discarding) is included in the matrix inversions used here.

The results of Figure 12 demonstrate that for certain interface representations, specifically r_1 and r_2 (i.e. all DoFs, and vertical z with x/y rotations) the transmissibility is able to attribute damage to the correct component (B), though notable level of damage is still predicted within A . This is likely due to small experimental errors in the repeated measurement of the baseline and damaged cases being amplified by the matrix inversion (note that this error amplification is generally greater for larger matrices, such as those used for r_1).

Importantly, representations r_3 and r_4 fail to correctly attribute the damage to B ; that is, the damage in B has a greater effect on the transmissibility of A than B . This result is particularly evident for r_4 where only a single vertical z DoF is included at each connection point. These results follow those of the ICC presented in Figure 11. This recapitulates the main result of this paper – without a sufficiently complete interface representation, transmissibility-based damage metrics are unable to robustly localise damage. That said, even with a complete interface representation experimental error can still lead to falsely identified damage.

Shown in Figure 13 are the ICCs for each of the representations, over the chosen frequency range, for the resiliently coupled case. These results suggest that all representations provide reasonable levels of completeness.

In fact r_1 and r_2 provide similar and reasonable levels of completeness, though over different frequency ranges.

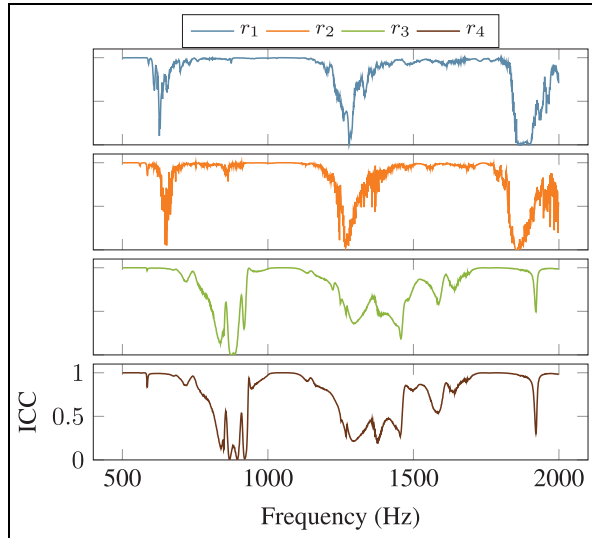


Figure 13. Interface completeness obtained for each representation r_n for the resiliently coupled case.

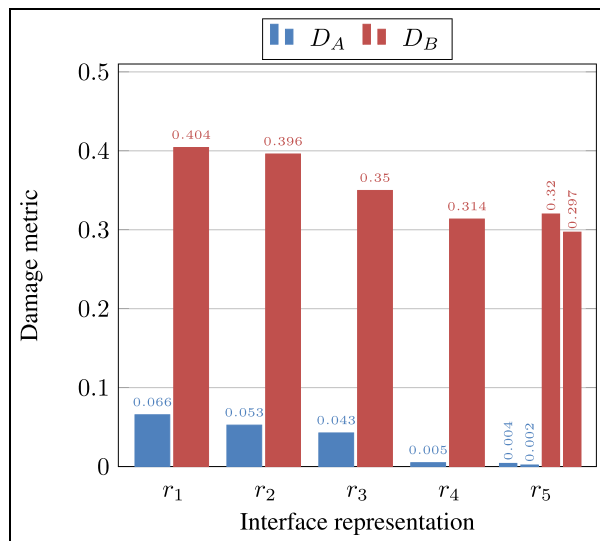


Figure 14. Single value damage metrics for sub-structures A and B (resiliently coupled with damage located in B) for different interface representations.

Shown in Figure 14 are the single value damage metrics obtained for A and B , whilst resiliently coupled, for the same interface representations as before. Note that in this case, the interface c was defined as that between A and the coupling element, such that component B now ‘includes’ the installed isolators. The results obtained for the resilient case are in stark contrast to those of Figure 12; for all representations, damage is correctly attributed to B , with minimal damage

predicted within A . This is on account of the weaker coupling between A and B ; fewer DoFs are generally required to capture the dynamics of a resilient interface, as in plane and rotational DoFs tend to contribute much less than for the rigid case.

Another interesting result from Figure 14 is the general downward trend of the damage metric (for both A and B) as the number of interface DoFs is reduced. Again, this is likely due to the reduced influence of experimental error, as the matrix inversions required reduce from 12×12 in r_1 to 2×2 in r_4 .

Conclusion

Transmissibility functions have been used widely within the SHM community over the past two decades. Compared to conventional FRFs (e.g. mobility), they are a) available using output-only methods, and b) have been shown to provide better localisation capabilities, though no definitive explanation for this latter feature has been offered. In the present paper we elucidate the origins of this capability; the blocking constraints present in the definition of both force and response transmissibility. Indeed, the (generalised) transmissibility, when defined between a *complete* set of interface DoFs and a set of remote points, becomes a sub-structural invariant; it is influenced only by damage located within that sub-structure. This unique property of sub-structural invariance is, however, reliant on the use of a complete interface representation, that is, a sufficient number of DoFs should be captured at the component’s separating interface. How many, and which DoFs will depend on the structure under study.

It was shown, through a series of numerical and experimental studies, that the completeness of an interface representation is directly correlated to the localisation accuracy of transmissibility-based damage metrics. It was further shown, that for the studies considered, incomplete representations can lead to damage being falsely attributed to the wrong sub-structure.

From these results we conclude that transmissibility-based metrics should not be relied upon, without sufficient understanding of the interface representation and its level of completeness. Furthermore, the present study raises the question whether knowledge of the interface completeness can be used to develop more robust transmissibility-based metrics that avoid the need for excessive instrumentation.

Acknowledgements

The authors would like to acknowledge the support of DSTL.

Declaration of conflicting interests

The author(s) declared no potential conflicts of interest with respect to the research, authorship, and/or publication of this article.

Funding

The author(s) received no financial support for the research, authorship, and/or publication of this article.

ORCID iD

Joshua WR Meggitt  <https://orcid.org/0000-0002-6665-2939>

References

1. Maia NM, Almeida RA, Urgueira AP, et al. Damage detection and quantification using transmissibility. *Mech Syst Signal Process* 2011a; 25(7): 2475–2483.
2. Rytter A. *Vibration based inspection of civil engineering structures*. PhD thesis, Aalborg University, Aalborg, Denmark, 1993.
3. Chesné S and Deraemaeker A. Damage localization using transmissibility functions: a critical review. *Mech Syst Signal Process* 2013; 38(2): 569–584.
4. Meggitt J and Moorhouse A. Finite element model updating using in-situ experimental data. *J Sound Vib* 2020a.
5. Meggitt JWR and Moorhouse AT. On the completeness of interface descriptions and the consistency of blocked forces obtained in situ. *Mech Syst Signal Process* 2020c; 145: 106850.
6. Moorhouse AT, Elliott AS and Evans TA. In situ measurement of the blocked force of structure-borne sound sources. *J Sound Vib* 2009; 325(4–5): 679–685.
7. Meggitt JWR. An introduction to the in-situ blocked force method for vibration source characterisation. Technical report, University of Salford 2022.
8. Bobrovnikskii Y. A theorem on representation of the field of forced vibrations of a composite elastic system. *Akusticheskij Zhurnal* 2001; 47(5): 586–590.
9. Lage YE, Neves MM, Maia NM, et al. Force transmissibility versus displacement transmissibility. *J Sound Vib* 2014; 333(22): 5708–5722.
10. Maia NM, Silva JM and Ribeiro AM. The transmissibility concept in multi-degree-of-freedom systems. *Mech Syst Signal Process* 2001; 15(1): 129–137.
11. Weijtjens W, De Sitter G, Devriendt C, et al. Operational modal parameter estimation of mimo systems using transmissibility functions. *Automatica* 2014; 50(2): 559–564.
12. Johnson TJ and Adams DE. Transmissibility as a differential indicator of structural damage. *J Vib Acoust* 2002; 124(4): 634–641.
13. Chen Q, Chan Y, Worden K, et al. Structural fault detection using neural networks trained on transmissibility functions. In: *Proceedings of the international conference on vibration engineering* 1994, pp. 456–646.
14. Zhang H, Schulz M, Naser A, et al. Structural health monitoring using transmittance functions. *Mech Syst Signal Process* 1999; 13(5): 765–787.
15. Ghoshal A, Sundaresan MJ, Schulz MJ, et al. Structural health monitoring techniques for wind turbine blades. *J Wind Eng Ind Aerodynamics* 2000; 85(3): 309–324.
16. Johnson TJ, Brown RL, Adams DE, et al. Distributed structural health monitoring with a smart sensor array. *Mech Syst Signal Process* 2004; 18(3): 555–572.
17. Caccese V, Mewer R and Vel SS. Detection of bolt load loss in hybrid composite/metal bolted connections. *Eng Struct* 2004; 26(7): 895–906.
18. Feng L, Yi X, Zhu D, et al. Damage detection of metro tunnel structure through transmissibility function and cross correlation analysis using local excitation and measurement. *Mech Syst Signal Process* 2015; 60: 59–74.
19. Maia NM, Almeida RA, Urgueira AP, et al. Damage detection and quantification using transmissibility. *Mech Syst Signal Process* 2011b; 25(7): 2475–2483.
20. Zhou YL, Cao H, Liu Q, et al. Output-based structural damage detection by using correlation analysis together with transmissibility. *Materials* 2017; 10(8): 866.
21. Zhang L, Lang ZQ and Papaelias M. Generalized transmissibility damage indicator with application to wind turbine component condition monitoring. *IEEE Trans Ind Electron* 2016; 63(10): 6347–6359.
22. Zhou YL, Figueiredo E, Maia N, et al. Damage detection and quantification using transmissibility coherence analysis. *Shock Vib* 2015.
23. Moorhouse AT, Evans TA and Elliott AS. Some relationships for coupled structures and their application to measurement of structural dynamic properties in situ. *Mech Syst Signal Process* 2011; 25(5): 1574–1584.
24. Haeussler M, Mueller T, Pasma E, et al. Component TPA: Benefit of including rotational degrees of freedom and over-determination. In: *Proceedings of the international conference on noise and vibration engineering*, Leuven, Belgium, 2020, pp. 7–9.
25. Sattinger S. Method for experimentally determining rotational mobilities of structures. *Shock Vib Bull* 1980; 50.
26. Meggitt J, Moorhouse A, Wienen K, et al. A framework for the propagation of uncertainty in transfer path analysis. *J Sound Vib* 2020; 483: 115425.
27. Fahy FJ and Walker J. *Advanced applications in acoustics, noise and vibration*. 2015.

Appendix

A Analysis of incomplete transmissibilities

In this section we present some further analysis regarding the influence of incompleteness on the transmissibility. In particular, we are interested in quantifying the influence of sub-structure B onto the transmissibility of sub-structure A , when only a subset of interface DoFs are considered.

To determine the contribution of individual sub-structures it is convenient to describe the transmissibility in terms of inverse quantities (e.g. stiffness, impedance or effective mass). Considering the coupled AB assembly in Figure 1(a), the equations of motion are,

$$\begin{pmatrix} \mathbf{f}_a \\ \mathbf{f}_c \end{pmatrix} = \begin{bmatrix} \mathbf{Z}_{Aaa} & \mathbf{Z}_{Aac} \\ \mathbf{Z}_{Aca} & \mathbf{Z}_{Acc} + \mathbf{Z}_{Bcc} \end{bmatrix} \begin{pmatrix} \mathbf{u}_a \\ \mathbf{u}_c \end{pmatrix} \quad (\text{A1})$$

where \mathbf{Z}_{Nij} is a sub-structure (dynamic) stiffness matrix. Note that the interface stiffness matrix is represented here by the summed interface stiffness matrices of sub-structures A and B , $\mathbf{Z}_{ABcc} = \mathbf{Z}_{Acc} + \mathbf{Z}_{Bcc}$.

By applying an appropriate blocking force at the interface c , we are able to enforce the constraint $\mathbf{u}_c = \mathbf{0}$ (and consequently $\mathbf{u}_b = \mathbf{0}$),

$$\begin{pmatrix} \mathbf{f}_a \\ -\mathbf{f}_{Ac} \end{pmatrix} = \begin{bmatrix} \mathbf{Z}_{Aaa} & \mathbf{Z}_{Aac} \\ \mathbf{Z}_{Aca} & \mathbf{Z}_{Acc} + \mathbf{Z}_{Bcc} \end{bmatrix} \begin{pmatrix} \mathbf{u}_a \\ \mathbf{0} \end{pmatrix}. \quad (\text{A2})$$

Note that this blocking force effectively removes the influence of sub-structure B . From the top row of Equation (A2) we obtain,

$$\mathbf{u}_a = \mathbf{Z}_{Aaa}^{-1} \mathbf{f}_a \quad (\text{A3})$$

which upon substitution into the second row yields,

$$-\bar{\mathbf{f}}_{Ac} = \mathbf{Z}_{Aca} \mathbf{Z}_{Aaa}^{-1} \mathbf{f}_a. \quad (\text{A4})$$

The matrix product in Equation (A4) may be interpreted as a generalised blocked force transmissibility. It relates an applied force \mathbf{f}_a at the internal DoFs a , to the blocked force necessary to constrain the interface DoFs c . It is entirely equivalent to the transmissibility of Equation (4),

$$\mathbf{T}_{Aca}^f = \mathbf{Z}_{Aca} \mathbf{Z}_{Aaa}^{-1} = \mathbf{Y}_{Ccc}^{-1} \mathbf{Y}_{Cca}. \quad (\text{A5})$$

The invariance of \mathbf{T}_{Aca}^f is clearly discernable here, since both \mathbf{Z}_{Aca} and \mathbf{Z}_{Aaa} are invariant properties of sub-structure A .

Let us now consider the coupled AB assembly in Figure 1(b), where the interface DoFs have been separated into known (c_i) and unknown (c_j) DoFs. After applying an appropriate blocking force at the known interface DoFs c_i , the equations of motion are

$$\begin{pmatrix} \mathbf{f}_a \\ -\bar{\mathbf{f}}_{Ac_i} \\ \mathbf{0} \end{pmatrix} = \begin{bmatrix} \mathbf{Z}_{Aaa} & \mathbf{Z}_{Aac_i} & \mathbf{Z}_{Aac_j} \\ \mathbf{Z}_{Ac_ia} & \mathbf{Z}_{Ac_ici} + \mathbf{Z}_{Bc_ici} & \mathbf{Z}_{Ac_ici} + \mathbf{Z}_{Bc_ici} \\ \mathbf{Z}_{Ac_ja} & \mathbf{Z}_{Ac_jci} + \mathbf{Z}_{Bc_jci} & \mathbf{Z}_{Ac_jcj} + \mathbf{Z}_{Bc_jcj} \end{bmatrix} \begin{pmatrix} \mathbf{u}_a \\ \mathbf{0} \\ \mathbf{u}_{c_j} \end{pmatrix}. \quad (\text{A6})$$

Table B1. Remote position coordinates. Bold value corresponds to the added mass location.

$A(x, y)$	$B(x, y)$
0.05, 0.10	0.50, 0.42
0.12, 0.75	0.60, 0.10
0.16, 0.35	0.85, 0.33
0.22, 0.54	0.80, 0.60
0.30, 0.6	0.45, 0.73

From the top row of Equation (A6) we obtain,

$$\mathbf{u}_a = \mathbf{Z}_{Aaa}^{-1} \mathbf{f}_a - \mathbf{Z}_{Aaa}^{-1} \mathbf{Z}_{Aac_j} \mathbf{u}_{c_j} \quad (\text{A7})$$

which upon substitution into the second row yields,

$$-\bar{\mathbf{f}}_{Ac_i} = \mathbf{Z}_{Ac_ia} (\mathbf{Z}_{Aaa}^{-1} \mathbf{f}_a - \mathbf{Z}_{Aaa}^{-1} \mathbf{Z}_{Aac_j} \mathbf{u}_{c_j}) + \dots (\mathbf{Z}_{Ac_ici} + \mathbf{Z}_{Bc_ici}) \mathbf{u}_{c_j} \quad (\text{A8})$$

or equivalently,

$$-\bar{\mathbf{f}}_{Ac_i} = \mathbf{T}_{Ac_ia}^f \mathbf{f}_a + (\mathbf{Z}_{ABc_ici} - \mathbf{Z}_{Ac_ia} \mathbf{Z}_{Aaa}^{-1} \mathbf{Z}_{Aac_j}) \mathbf{u}_{c_j}. \quad (\text{A9})$$

It is clear from Equation (A9) that by neglecting the DoFs c_j the relation between \mathbf{f}_a and $-\bar{\mathbf{f}}_{Ac_i}$ is no longer governed by a transmissibility alone; a second term, proportional to the response \mathbf{u}_{c_j} (a property of the coupled AB assembly), is present. This second term introduces two additional contributions to the blocked force. The first, $\mathbf{Z}_{ABc_ici} \mathbf{u}_{c_j}$, describes the blocking force present at the known interface DoFs c_i due to motion at the unknown DoFs c_j . The second, $\mathbf{Z}_{Ac_ia} \mathbf{Z}_{Aaa}^{-1} \mathbf{Z}_{Aac_j} \mathbf{u}_{c_j}$, describes the blocking force present due to motion at a , itself induced by the motion at c_j .

B Details on numerical plate model

The numerical plate was modelled using a simply supported modal summation model with a total of $n_m = 60^2$ modes included.²⁷ The plate's geometry was $L_X = 1$ m (length), $L_Y = 0.8$ m (width) and $L_Z = 0.005$ m (thickness). Its Young's modulus, density and loss factor were set, respectively, to $E = 200 \times 10^9 \text{ Nm}^{-2}$, $\rho = 7000 \text{ kg m}^{-3}$ and $\eta = 0.05$. The coordinates of the remote A and B positions are detailed in Table B1. The interface points share a common x coordinate of 0.35 m. Their y coordinates are such that each point is equally spaced from its neighbouring points or plate edge, as illustrated in Figure 2.